

Kimberly B. Colas,¹ Arthur T. Motta,¹ Mark R. Daymond,² Matthew Kerr,² and Jonathan D. Almer³

Hydride Platelet Reorientation in Zircaloy Studied with Synchrotron Radiation Diffraction

ABSTRACT: Hydrogen ingress into zirconium alloy fuel cladding in light water reactors can degrade cladding performance as a result of the formation of brittle hydrides. In service, hydrides normally precipitate in the circumferential direction and are homogeneously distributed through the cladding thickness in ideal cases. However, temperature and stress gradients in the cladding can promote hydrogen redistribution. This hydrogen redistribution is responsible for the formation of hydride rims, dissolution, and reorientation of hydride precipitates and for the formation of brittle hydrides at stress concentration locations, all of which can reduce cladding resistance to failure. Thus, it is crucial to understand the kinetics of hydride dissolution and precipitation under load and at temperature. Studies of hydrogen behavior in zirconium alloys are normally performed post facto, which causes them to suffer both from a scarcity of data points and from the confounding effects of studying hydrides at room temperature that might be dissolved at higher temperature. In the current study, we have used synchrotron radiation diffraction to study the kinetics of hydride precipitation and dissolution in situ (under load and at temperature). Samples of hydrided Zircaloy-4 were examined in transmission by using 80 keV synchrotron radiation while undergoing heating and cooling in a furnace. Temperatures ranged from 20 to 550°C, and loads from 75 to 100 MPa were applied. The hydrides dissolved and reprecipitated in a different orientation when sufficiently high loads were applied. Through careful study of the intensities and full-width half maxima of the diffraction peaks as a function of time, load, and temperature, it was possible to identify the characteristic diffraction patterns for the reoriented hydrides so that the kinetics of dissolution, reprecipitation, and orientation of the hydrides could be followed. The analysis of the diffraction patterns allowed a detailed understanding of the kinetics of hydride evolution under temperature and stress, as presented in this work.

KEYWORDS: zirconium hydrides, reorientation, synchrotron radiation diffraction, strain broadening

Introduction

Zirconium alloys used for reactor core structural components and fuel cladding can be embrittled by the presence of zirconium hydride precipitates, which form as a result of hydrogen ingress due to the phenomena associated with reactor corrosion and water radiolysis [1]. The hydrides observed in fuel cladding exposed to reactor environment are most often face-centered-cubic δ -hydrides ZrH_x (where $x \sim 1.6$) [2], although γ - and ϵ -hydrides are occasionally observed [3,4]. δ -hydrides are shown by electron microscopy to be platelet-shaped and to form with a near $(111)_\delta \parallel (0002)_\alpha$ orientation relationship with the α -zirconium matrix [5]. The larger hydride plates observed optically have been reported to be constituted of a stacking of several of these smaller platelets [6]. The orientation and morphology of these larger hydrides plates are primarily dependent on the zirconium matrix microstructure, thermal history, and stress state (both applied and residual). During drying and storage, high temperatures (of up to 400°C) can be attained, and part of the hydride population can dissolve and reprecipitate with a different orientation. In the absence of an applied stress field, hydride precipitation is dependent on the texture of the zirconium matrix and is governed by the orientation of the last compressive step in the thermo-mechanical treatment which normally results in planar or “circumferential” hydrides [7]. However, the presence of a sufficiently high applied tensile stress field (typically starting at around 80 MPa) during cooling causes the hydride platelets to precipitate preferentially perpendicular to the applied tensile stress direction. The level of applied stress required for hydride reorientation depends on the microstructure, prior processing, and hydrogen concen-

Manuscript received February 8, 2010; accepted for publication October 23, 2010; published online December 2010.

¹ Dept. of Mechanical and Nuclear Engineering, Penn State Univ., University Park, PA 16802.

² Dept. of Mechanical and Materials Engineering, Queen’s Univ., Kingston, ON K7L 2N8, Canada.

³ Advanced Photon Source, Argonne National Laboratory, Argonne, IL 60439.

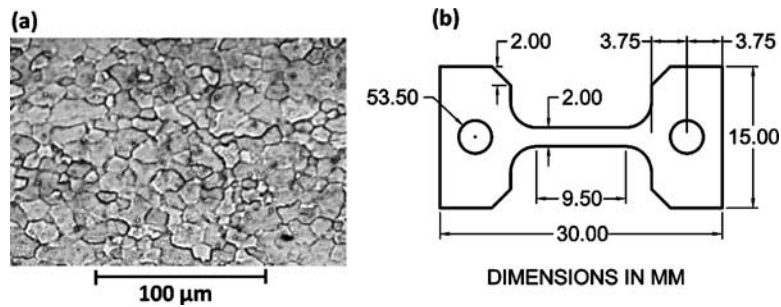


FIG. 1—(a) Optical image of grain structure of the cross section of as-received material and (b) sample dimensions. The sample thickness is 0.5 mm.

tration as well as thermo-mechanical loading [8]. Because of this, concern has arisen that such hydride reorientation could occur during dry storage of spent fuel, especially in the case of high burn-up and corresponding high hydrogen concentrations, causing the fuel cladding to become more brittle. As a result, an understanding of hydride reorientation phenomena is of great technological importance.

Most analyses of changes in hydride microstructure have been performed post facto, at room temperature, and after applied stress has been removed. Typically, the hydride orientation is determined by using metallography before and after the heating/loading cycles [9–11]. It would be of great interest to combine the post facto metallographic techniques with in situ measurements of hydride reorientation. Recent studies using high energy synchrotron X-ray diffraction have demonstrated that it is possible to observe zirconium hydride phases and to distinguish the crystallographic nature of the hydride phases present (δ from γ , for example) [12]. The strain measurements of zirconium hydrides embedded in a zirconium alloy matrix have also been conducted, both in the bulk and at notch tips [13,14]. Synchrotron measurements have proven to be reliable in measuring internal strains, comparing favorably to measurements made at neutron diffraction sources [15,16]. The advantage of a synchrotron source is that these measurements can be made with shorter exposure times and with higher resolution, owing to the high photon flux available. In addition, high energy beams allow the examination of thicker samples.

The in situ synchrotron diffraction experimental set-ups such as the one presented in this paper could be used to study many essential features of the behavior of hydrides under temperature and stress. In this study, high energy X-rays were used in transmission to obtain diffraction data while the sample was loaded at temperature. These techniques were used to observe hydride reorientation in the matrix of zirconium alloys during heating and cooling cycles under stress. Further experiments could be conducted involving full reorientation of the entire population of hydrides, multiple temperature cycles to study the possible memory effect on hydride precipitation, and/or materials with composition and textures differences. The work on the determination of the terminal solid solubility of hydrogen using this technique has also been performed and will be published elsewhere. The aim of this study is to follow the process of hydride reorientation in situ by using synchrotron X-ray diffraction.

Experimental Procedures

Material and Sample Preparation

Zircaloy-4 base alloy furnished by Western Zirconium was used in this study. The material was in the form of a 0.5 mm thick sheet in the recrystallized condition. An optical metallograph of the as-received material is shown in Fig. 1(a). The grains are equiaxed and their diameter is $\sim 10 \mu\text{m}$. These samples were machined to a tensile “dog-bone” shape with a reduced width at the gage section to obtain stress concentration, as seen in Fig. 1(b). The tensile axis of the sample is aligned with the rolling direction. The sample dimensions are detailed in Fig. 1(b).

These samples were hydrogen-charged by high temperature gas diffusion, for which several steps were needed. First, the native oxide layer present on the surface of the samples was removed by dipping the samples for 1 min in a solution of 1 part hydrofluoric acid, 10 parts nitric acid, and 10 parts H_2O . Second, by using an electron-beam evaporator, a thin layer of nickel (200 Angstroms thick) was deposited into the sample surface to prevent the native oxide from reforming while still allowing hydriding [17]. The samples

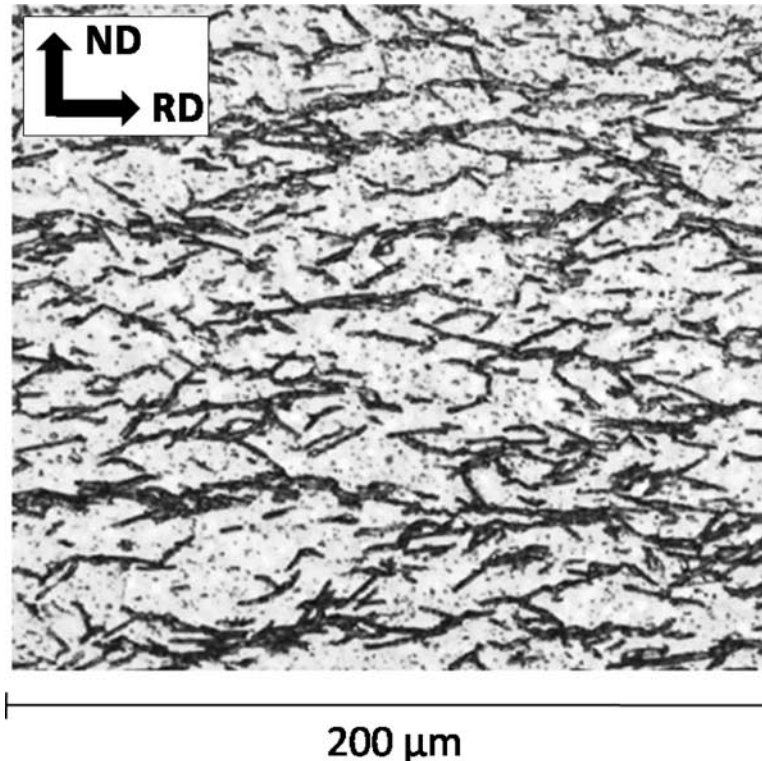


FIG. 2—Optical metallograph of a Zircaloy-4 sample hydrided to 525 wt ppm. The sample orientation is represented by the black arrows.

were then hydrogen-charged in a vacuum furnace using a mixture of 12 % hydrogen and 88 % argon, introduced at 450°C. Several temperature cycles were necessary to charge to the desired levels of hydrogen. The total time at 450°C was 3 h, so no significant recrystallization occurred [18]. The final hydrogen contents of the sample were measured by hot vacuum extraction performed by Luvak, Inc. The samples used in this study were charged to 525 ± 10 wt ppm of hydrogen.

After hydrogen-charging, metallography was performed to characterize the hydride morphology. The samples were mounted in a cross section in epoxy casts and mechanically polished to 1200 grit silicon carbide paper, followed by chemical etching using the same solution used for oxide layer removal. This solution preferentially etched the zirconium hydrides, which allowed their observation by using optical microscopy. One example of such an examination is shown in Fig. 2 for a sample with 525 wt ppm of hydrogen. It is seen that in the initial state, the hydride platelets (dark lines) are mostly perpendicular to the normal direction (ND), and thus they are in-plane, or circumferential hydrides. The hydride orientation was estimated using image analysis. Each individual particle was counted as a circumferential hydride, a mixed hydride, or a radial hydride. The circumferential hydrides were those whose normals were oriented between 0° and 40° from the ND (or radial direction for a cladding tube), the mixed hydrides were those whose normals were oriented between 40° and 65° from the ND, and the radial hydrides were those whose normals were oriented between 65° and 90° from the ND [19].

Temperature and Load

While being analyzed by synchrotron X-ray diffraction, the samples underwent heating and cooling cycles under load. The samples in this study were heated up to 550°C in order to dissolve all the hydrides in the matrix (the solubility of hydrogen in zirconium at 550°C is about 640 wt ppm [20]), then cooled back to room temperature under tensile load applied in the rolling direction (RD). An example of a typical temperature/load run is shown in Fig. 3. Each sample was cycled only once, and the time at maximum temperature (550°C) was at most 15 min, so no significant grain growth or recrystallization has occurred [18]. The testing temperature was controlled by using an optical furnace and the sample temperature was monitored by using K-type thermocouples, which were spot welded into the sample surface. The MTS[®] frame used for tensile testing allowed the computer monitoring of the applied load and the displacement or

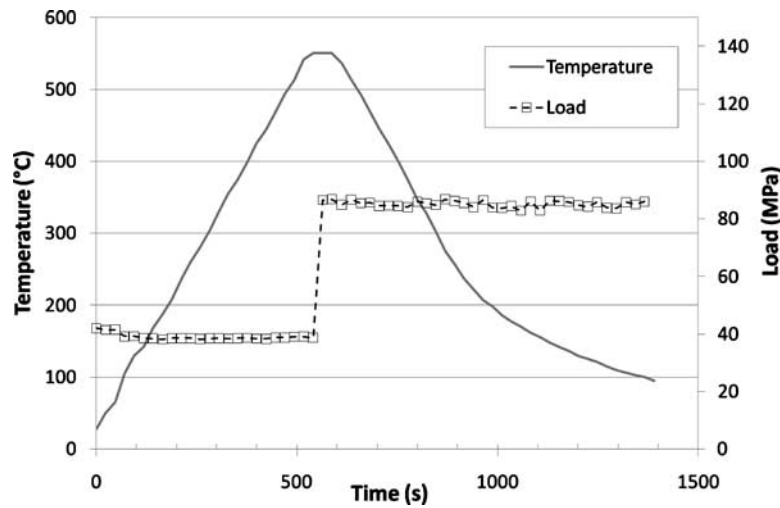


FIG. 3—Typical *in situ* heat/load cycle.

the displacement rate of the crosshead. The applied (engineering) stress was determined by dividing the applied force by the initial gage cross section.

Synchrotron Data Acquisition

The X-ray diffraction examination of the samples was conducted at beamline 1-ID at the Advanced Photon Source at Argonne National Laboratory with the objective of observing the dissolution and precipitation kinetics of the zirconium hydrides. The experimental geometry is described in Fig. 4. The experiments were conducted in transmission geometry by using 80 keV X-rays ($\lambda=0.015$ nm) and a beam size of 0.3×0.3 mm² [21]. This experimental set-up allows the observation of the hydride diffracted intensity as the sample is heated or cooled under load. A high-speed area detector (1 s time resolution) was used to collect diffraction patterns, allowing the full diffraction rings to be recorded. Because the data was obtained in transmission, the diffraction signal is averaged over the full sample thickness. The diffraction rings can be integrated over their full circumference or over selected angular ranges to obtain the diffracted intensity from planes oriented in particular directions of interest relative to the macroscopic sample directions. A typical diffraction pattern integrated over the full circumference for a sample with 525 wt ppm of hydrogen is presented in Fig. 5. For this study, it was chosen to integrate the diffraction rings

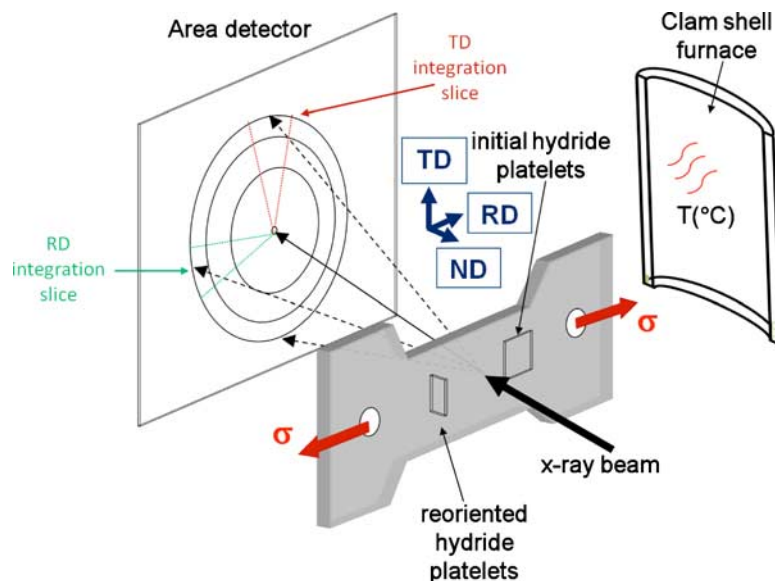


FIG. 4—Experimental set-up of beamline 1-ID. The integration directions are indicated on the area detector.

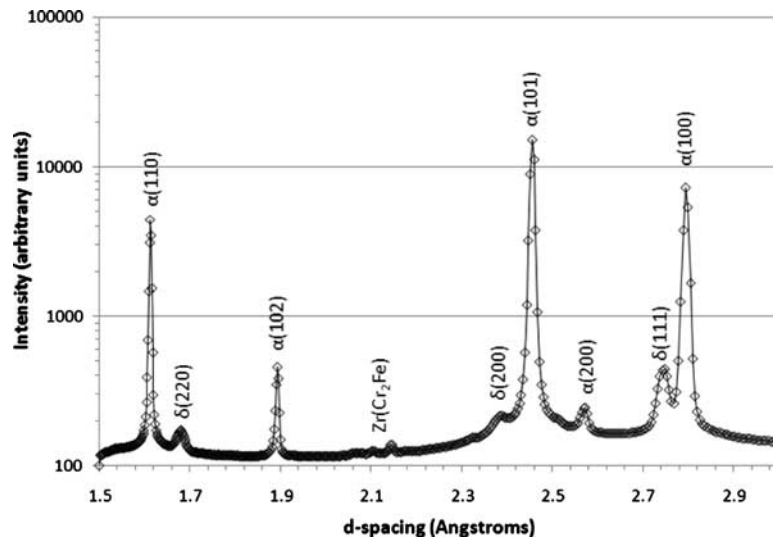


FIG. 5—X-ray diffraction pattern of a Zircaloy-4 material sample with 525 wt ppm of hydrogen (logarithmic scale).

around specific orientations close to the RD and transverse direction (TD) as illustrated in Fig. 4. The diffraction signals from the “TD” come from crystallographic planes with normals parallel to the TD (within a $\pm 10^\circ$ angular range around the TD) and diffraction signals in the “RD” come from crystallographic planes, which have their normals parallel to the RD (in a $\pm 10^\circ$ angular range around the RD).

Synchrotron Data Analysis

The typical raw data obtained during this experiment was in the form of ten two-dimensional images successively obtained using the plate detector for each diffraction pattern recorded (this was necessary to avoid saturation of the detector for the high intensity Zr peaks while still obtaining good statistics for the weak hydride peaks). The ten images were summed and averaged to create the diffraction pattern. Using a computer routine, the full diffraction rings were integrated over four specific angular ranges of $\pm 10^\circ$ around 0° , 90° , 180° , and 270° . The data from the angular ranges obtained was then averaged (average of the sum of 0° and 180° ranges (RD) and average of the sum of 90° and 270° ranges (TD)) and reduced to a file suitable for analysis. The diffraction peaks obtained were then analyzed by using a single peak fitting routine available within the GSAS/Rawplot[®] program [22]. General structure analysis system (GSAS) is primarily a Rietveld refinement program that can fit all the different parameters that would affect peak height, shape and position. Rawplot is a subroutine that allows faster fitting of only the peak shape, position and intensity of the raw data. The peaks were fitted using a pseudo-Voigt function, which is a convolution of Gaussian and Lorentzian peak shapes. In the GSAS fitting routine, the Lorentzian full-width at half maximum (FWHM) was kept constant, while the Gaussian FWHM was allowed to vary; the Lorentzian FWHM is normally associated with instrumental broadening (which was determined independently in this study by using a calibration powder to be 0.22×10^{-2} degrees in 2θ), whereas the Gaussian FWHM is normally associated with sample broadening, such as size or strain broadening [23]. The background was fitted over the entire diffraction range by using a third-degree polynomial function and subtracted from the data prior to fitting. This allowed iterative fitting of the diffraction peaks to obtain (i) the peak positions, (ii) the integrated intensity, and (iii) the Gaussian FWHM of the refined peaks. The instrumental broadening was determined by running a ceria standard powder used as a reference for broadening and subtracted in quadrature from each peak to isolate the sample contribution to line broadening. When measured under stress, the peak positions can be related to the elastic strain of the diffracting crystallites, while peak broadening can originate from various causes, including size broadening, inhomogeneous elastic strain, and from plastic strain broadening [23].

Results and Discussion

As explained in the previous section, the analysis of the diffraction data yields peak positions (and thus d -spacing), integrated intensities, and FWHM for each peak. As mentioned above, these values can be

TABLE 1—Measured and expected peak positions for a Zircaloy-4 sample with 525 wt ppm of hydrogen (for two integration directions) for an X-ray energy of 80 keV. PDF stands for powder diffraction file, which serve as a reference for our phases [2].

Phase	HKL	Integration Direction	Powder Diffraction Files Values (°)	Experimental 2θ (°)	Difference (%)
α-Zr (PDF number: 5-0665)	100	TD	3.1461	3.1460	−0.0032
		RD	3.1461	3.1447	−0.0445
δ-hydride (PDF number: 34-0649)	111	TD	3.1894	3.2032	0.4327
		RD	3.1894	3.2030	0.4264
α-Zr (PDF number: 5-0665)	002	TD	3.4213	3.4191	−0.0643
		RD	3.4213	3.4211	−0.0058
α-Zr (PDF number: 5-0665)	101	TD	3.5800	3.5800	0.0000
		RD	3.5800	3.5774	−0.0726
δ-hydride (PDF number: 34-0649)	200	TD	3.6818	3.6877	0.1602
		RD	3.6818	3.6853	0.0951
α-Zr (PDF number: 5-0665)	102	TD	4.6484	4.6460	−0.0516
		RD	4.6484	4.6446	−0.0817
δ-hydride (PDF number: 34-0649)	220	TD	5.2098	5.2352	0.4875
		RD	5.2098	5.2334	0.4530
α-Zr (PDF number: 5-0665)	110	TD	5.4486	5.4513	0.0496
		RD	5.4486	5.4484	−0.0037

obtained by integration over the full diffraction ring or along portions of the ring oriented along particular directions. As a sample is heated and cooled under load, diffraction patterns are constantly recorded, enabling us to observe each of the parameters mentioned above as a function of time. The evolution of the above parameters with time allows us to follow the evolution of strain and stress of the phases present as a function of temperature and applied load. It should be noted, however, that the strain (and resulting stress) is calculated from the d -spacing shift and peak broadening and is not directly measured in our experiment.

X-Ray Diffraction Patterns

The diffraction pattern presented in Fig. 5 results from integration over the full diffraction ring of a sample containing 525 wt ppm of hydrogen. The α-zirconium and δ-hydride peaks were indexed using expected d -spacing values from the powder diffraction files indicated in Table 1 from Ref 2. Three δ-hydride peaks $(111)_\delta$, $(200)_\delta$, and $(220)_\delta$ and five α-zirconium peaks are observed. For the zirconium matrix, the intensity of the $(002)_\alpha$ peak is small compared to that of the $(100)_\alpha$ and $(101)_\alpha$ peaks (the prism planes and the pyramidal planes, respectively). This results from the basal texture created upon cold rolling, causing the basal poles to be preferentially aligned along the ND, and thus not in a strong diffraction condition in our transmission set-up. Table 1 shows a comparison of the peak positions determined from the experiment and those from the respective powder diffraction files. The α-zirconium peaks correspond well to the powder diffraction files, to the fourth significant digit, while the δ-hydride peaks agree to the third significant digit. The difference between the observed and theoretical peak position in the hydrides could indicate that the hydrides are elastically strained in the compressive direction due to the thermal expansion mismatch between the hydrides and the α-zirconium matrix or that the hydrides have a slightly different stoichiometry than that reported in the literature.

If it is assumed that such a d -spacing change is caused by elastic strain, it is possible to estimate the stresses. When integrating the diffraction data obtained for this sample along the two particular directions, TD and RD, we obtain information on planes that are oriented perpendicular to these directions. Figure 6 shows the diffraction patterns integrated over the TD and RD for the sample shown in Fig. 5 (525 wt ppm of hydrogen). Only the 2θ region encompassing the $(111)_\delta$ and the $(100)_\alpha$ peaks is shown. The expected peak positions from Ref 2 are represented by the solid vertical lines. While the zirconium matrix peak is close to the expected peak position, the δ-hydride peak is shifted towards a lower d -spacing, suggesting that the hydrides precipitate particles are under a compressive strain. This is true both for hydrides oriented in the TD and the RD. The strain can be calculated from this difference in d -spacing by the following formula:

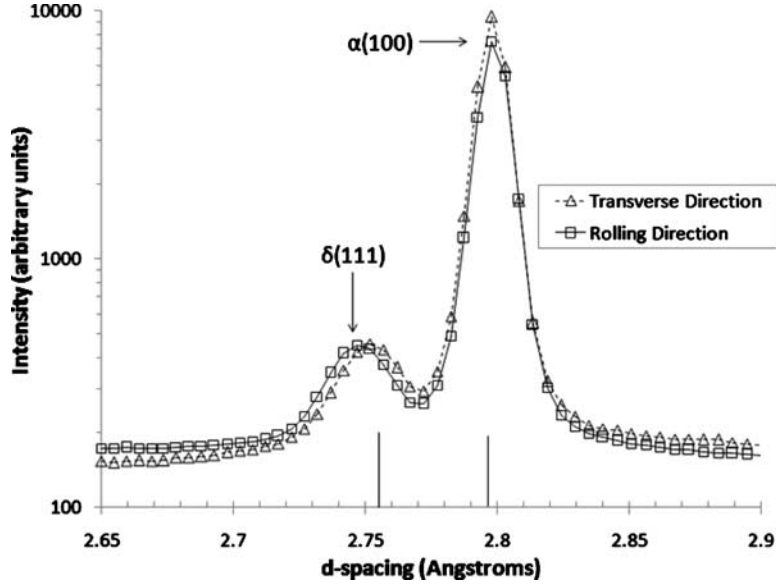


FIG. 6—X-ray diffraction pattern of the two integration slices of a Zircaloy-4 sample with 525 wt. ppm of hydrogen (respective TD and RD angles of $\pm 10^\circ$). The expected peak position for $\delta(111)$ and $\alpha(100)$ are represented by the solid vertical lines.

$$\varepsilon = (d_{\text{measured}} - d_{\text{PDF}})/d_{\text{PDF}} \quad (1)$$

where:

ε = strain,

d_{measured} = d -spacing measured from X-ray diffraction, and

d_{PDF} = d -spacing reported in Ref 2.

For the TD we find $\varepsilon_{\text{TD}} = (2.752 - 2.76)/2.76 = -2.9 \times 10^{-3}$, and for the RD we find $\varepsilon_{\text{RD}} = (2.747 - 2.76)/2.76 = -4.7 \times 10^{-3}$. Using the values of ~ 100 GPa for the elastic constant of the δ -hydride [24] and ~ 0.322 for Poisson's ratio for the hydrides [25], the stresses were calculated in the two directions based on a tri-axial stress state. Using the plane strain assumption to account for the condition in the un-measured ND direction, we obtain $\sigma_{\text{TD}} = 740$ MPa in compression in the TD and $\sigma_{\text{RD}} = 870$ MPa in compression in the RD. For a plane stress condition, we find $\sigma_{\text{TD}} = 490$ MPa in compression in the TD and $\sigma_{\text{RD}} = 630$ MPa in compression in the RD. The actual stress state in the hydrides will be somewhere between the values obtained for the assumptions of plane stress and plane strain. Given the geometry of the hydrides platelets and the preferential orientation relationship between the hydrides and the matrix in the ND, we expect the hydrides to be closer to a plane strain condition than plane stress. Given the plane strain assumption, we obtain a maximum stress component of 870 MPa (in compression) that can be compared to the value of ~ 800 MPa obtained by Kerr et al. for hydride fracture under a tensile applied load [26]. To compare the measured values with a yielding condition, we calculate the von Mises equivalent stress for a plane strain assumption (308 MPa) and for a plane stress assumption (570 MPa), both are somewhat below the hydride yield stress measured by Puls et al. of ~ 500 – 800 MPa for hydride plasticity at room temperature using microhardness indentation [24].

A compressive stress state is expected for the hydrides since under stress-free conditions, since the hydride phase is less dense than the zirconium matrix from which it is formed (i.e., undergoes a volume expansion relative to the matrix). The fact that the hydride planes are slightly more stressed in the RD than in the TD could be due to the difference in the basal plane fraction in these two directions. If a direction contains a higher percentage basal poles aligned with it (within $\pm 10^\circ$), then the thermal expansion coefficient will be different in this direction compared to the other directions due to the anisotropic properties of zirconium [18], which could lead to small differences in the compression of the hydride planes as they precipitate upon cooling. In our sample, there is a higher fraction of basal poles parallel to the RD (typical recrystallized texture [18]), thus leading to a larger thermal expansion coefficient and to higher compressive strains in the hydride in that direction.

The observation of the evolution of peak position and FWHM has been carried out systematically for

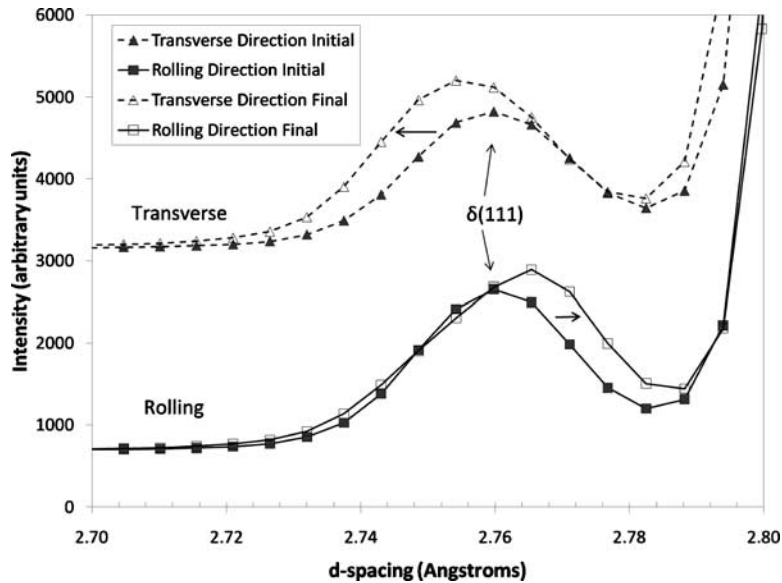


FIG. 7—Diffraction patterns of a sample with 525 wt ppm of hydrogen at the initial state and after loading at 75 MPa (no reorientation). Close-up on the $\delta(111)$ hydride peak.

samples that showed reoriented hydrides after thermal cycling under load and for samples that did not. Figures 7 and 8 compare the $(111)_\delta$ and $(220)_\delta$ hydride peaks for a sample that was heated and cooled under an applied tensile load of 75 MPa along the RD (no reorientation). In Fig. 7, it is observed that the $(111)_\delta$ peaks in the TD and the RD are initially of the same width and located approximately at the same peak position. After applying load in the RD, the $(111)_\delta$ peak in the RD appears to have shifted to a larger d -spacing, which is consistent with the fact that the planes in the RD are in tension. On the contrary, the planes in the TD have shifted towards a smaller d -spacing, implying that those planes are in compression. This is consistent with the fact that as a tensile load is applied in the RD, Poisson's ratio implies that the planes perpendicular to the RD (such as the TD planes) would be compressed. The same behavior is observed in the $(220)_\delta$ planes (Fig. 8). The RD planes shift to larger d -spacing (and thus they are in tension), while the TD planes shift towards a smaller d -spacing (and thus are in compression). It should also be noted that in their final state, we also observe a broadening of $(111)_\delta$ and $(220)_\delta$ RD peaks relative to the initial value but not of the peaks in the TD. This is most likely due to non-uniform strain broadening, as discussed below.

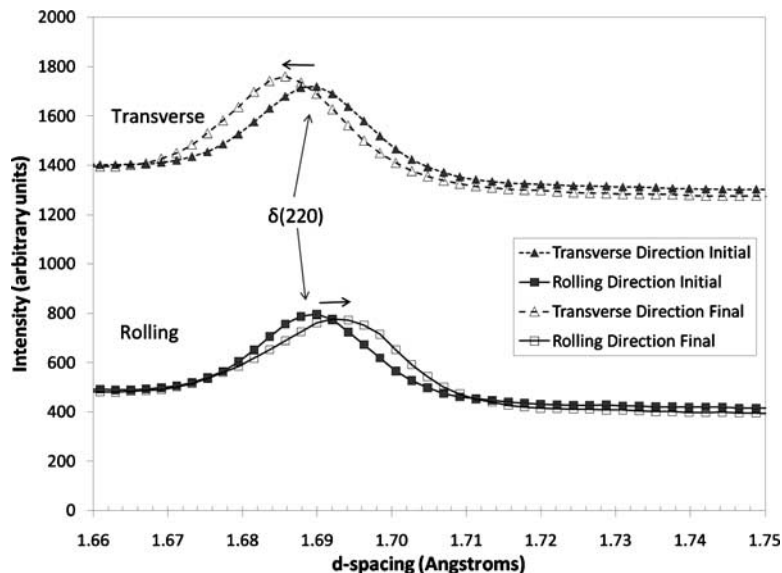


FIG. 8—Diffraction patterns of a sample with 525 wt ppm of hydrogen at the initial state and after loading at 75 MPa (no reorientation). Close-up on the $\delta(220)$ hydride peak.

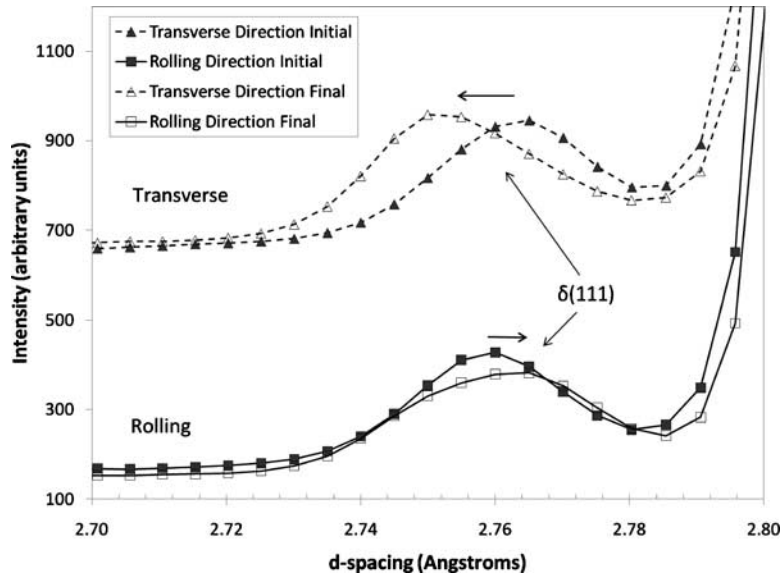


FIG. 9—Diffraction patterns of a sample with 525 wt ppm of hydrogen at the initial state and after loading at 85 MPa (with reorientation). Close-up on the $\delta(111)$ hydride peak.

Figures 9 and 10 compare the diffraction patterns of two hydride peaks for a sample that was heated and cooled under an applied load of 85 MPa and that shows reoriented hydrides (as explained above, the reorientation has been characterized by image analysis, an image of the micrograph showing reorientation can be seen in Fig. 15). In Fig. 9, we can see that initially the $(111)_\delta$ peaks from the TD and the RD have the same width and approximately the same peak position (the slight shift could be due to residual stresses in the matrix that affected the hydrides as they precipitated). After the thermal cycle under load in which the hydrides were dissolved and reoriented, we observe that the RD peak has shifted to the tension side (larger d -spacing) and the TD peak has shifted to the compression side (smaller d -spacing), which is consistent with an applied tensile load in the RD. In addition, the RD peak is much broader after reorientation than before, whereas the TD peak width has not changed. In Fig. 10, the evolution of the $(220)_\delta$ peak is shown before and after reorientation. The same type of shift previously seen in Fig. 9 is observed, with the RD peak shifting to a higher d -spacing and the TD peak shifting to a lower d -spacing. In this figure, however, the TD peak broadens significantly, whereas the RD peak has the same width before and

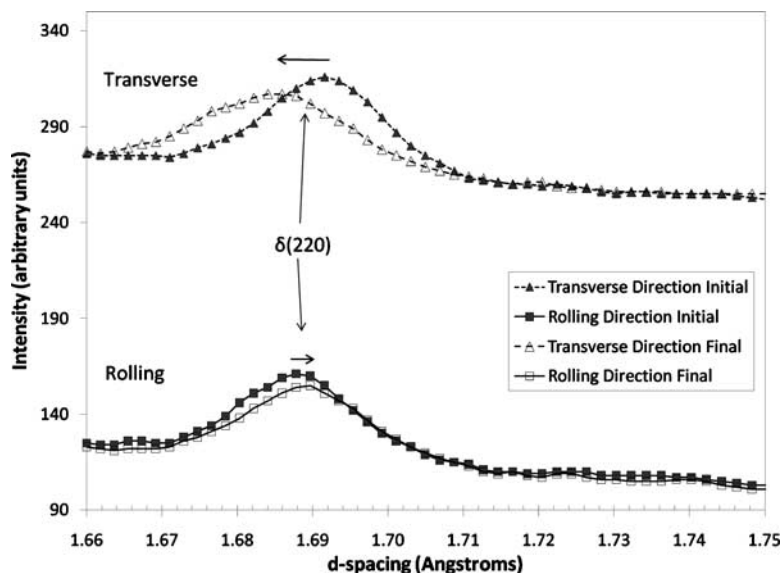


FIG. 10—Diffraction patterns of a sample with 525 wt ppm of hydrogen at the initial state and after loading at 85 MPa (with reorientation). Close-up on the $\delta(220)$ hydride peak.

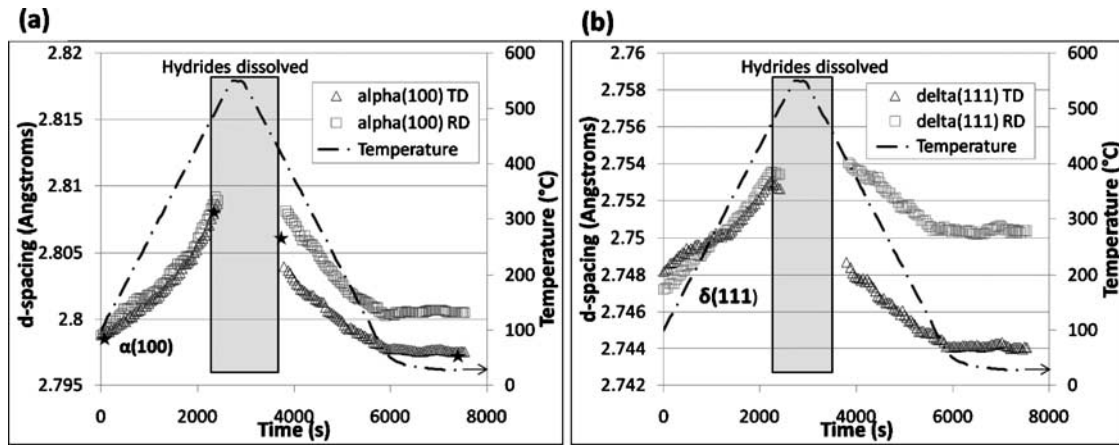


FIG. 11—The d -spacing of (a) $\alpha(100)$ and (b) $\delta(111)$ peaks for a Zircaloy-4 sample with 520 wt ppm of hydrogen for hydrides precipitated under 75 MPa applied load in the RD without reorientation (the expected thermal expansion stars come from Ref 24).

after reorientation. The observed peak broadening is attributed to different strains in hydrides that are reoriented compared to strains in hydrides that are not reoriented, as discussed in more detail below.

Evolution of d -Spacing with Time and Temperature

Recording data while heating and loading enables us to observe the evolution of selected parameters with time and temperature. Figure 11(a) and 11(b) shows the evolution of the d -spacing of the $(100)_\alpha$ peak and the $(111)_\delta$ peak for both integration directions for a sample heated and cooled under an applied load of 75 MPa. Factors influencing the lattice parameter include the temperature (thermal expansion), elastic stress/strain, and chemical composition. In the left-hand side of Fig. 11(a) and Fig. 11(b) (between 0 and 3000 s), the temperature steadily increases (at $0.2^\circ\text{C}/\text{s}$), which entails an increase of the d -spacing of the zirconium peaks by thermal expansion. Some expected points for the thermal expansion of the zirconium peaks [27] are plotted as stars for reference. Once at 550°C (around 3300 s), the tensile load is applied in the RD. When the load is applied, the RD peaks of both the zirconium and the hydride shift to a larger d -spacing, whereas the TD peaks of both phases shift to a smaller d -spacing. The shift away from the initial value of the hydride planes in the TD and the RD is $\sim 3.1 \times 10^{-3}$ Å. That of the zirconium planes in the TD and the RD is $\sim 1.5 \times 10^{-3}$ Å.

In Fig. 12, the same graphs shown in Fig. 11 are plotted for a sample that showed partial reorientation after being loaded at 85 MPa during cooling. The $(100)_\alpha$ and $(111)_\delta$ peaks behave similarly, as shown in Fig. 11: When the load is applied, the RD peaks shift to a larger d -spacing than initially, whereas the TD peaks shift to a smaller d -spacing than initially. The previous observations are confirmed by Fig. 13 where the same plots as in Figs. 11 and 12 are shown for a sample partially reoriented under 100 MPa load. In this case, we observe the same expected behavior for the zirconium peaks and for the hydride peaks. The last point of the graphs (after 1500 s) was recorded under zero applied load. We see that the hydride peaks are still shifted with respect to their initial peak position, indicating that this difference in strain is caused by permanent strain in the hydrides rather than by elastic stress from the applied load.

Intensity and Full-Width at Half Maximum Evolution with Time and Temperature

Observing the evolution of the integrated intensity and the FWHM for the $(111)_\delta$ hydride peaks with time and temperature can give additional information on the dissolution and precipitation of hydrides and on the broadening of the peaks. The evolution of the FWHM and the integrated intensity of the $(111)_\delta$ is presented in Fig. 14 for both TD and RD as a function of time for a sample heated and cooled under 75 MPa applied load. In this case, the hydride particles did not undergo reorientation. The temperature curve is shown as a dotted line, linked to the right-hand ordinate axis. The tensile load was applied in the RD once the sample temperature reached 550°C as shown in the bottom of the figure and most of the hydrides were dissolved. The load was kept constant thereafter. The metallographs of the cross section of the sample taken before and after the experiment are also shown in Fig. 14 (it should be noted that metallography was

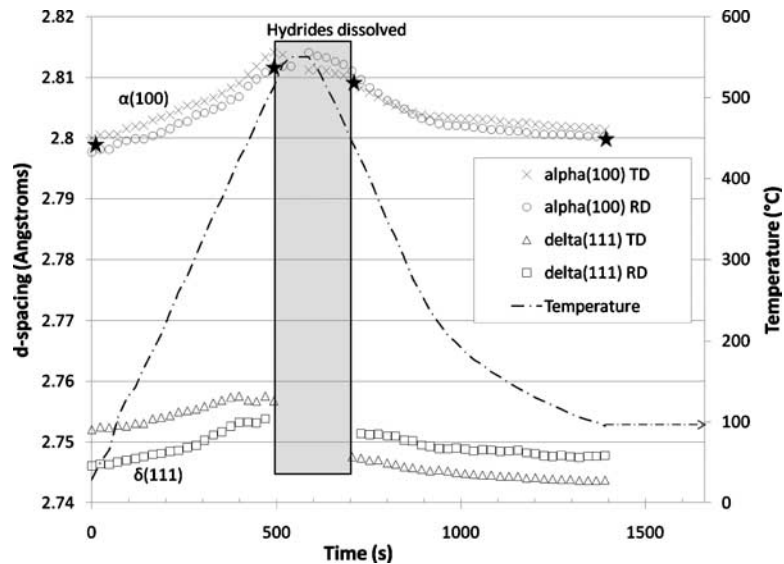


FIG. 12—The d -spacing of $\alpha(100)$ and $\delta(111)$ peaks for a Zircaloy-4 sample with 525 wt ppm of hydrogen cooled under 85 MPa applied load in the RD (the stars indicate the expected thermal expansion stars come from Ref 24). This cycle resulted in hydride reorientation.

performed on the exact same sample before and after the X-ray diffraction experiment; after the first metallographic observation, the sample was repolished to remove any effect from etching). On both of these metallographs, the hydride platelets are perpendicular to the ND, confirming that no hydride reorientation has occurred. In this figure, we can follow the dissolution of the hydride particles as the hydride peak intensity curve decreases as the temperature reaches $\sim 550^{\circ}\text{C}$ and returns to higher values upon cooling.

The examination of the changes in the $(111)_{\delta}$ peak FWHM can be related to strain or size broadening. Initially, the FWHM for both TD and RD are similar (as also shown in Fig. 7). When the hydrides start to dissolve, the $(111)_{\delta}$ hydride peak FWHM diminishes. This could be because since the hydrides are smaller, they are less strained in the zirconium matrix or because the most strained hydrides dissolve preferentially. The shape of the hydride particles dissolving could also be changing, leading to a lower strain on the hydride planes. When cooling under load, as the hydride particles reprecipitate, the FWHM increases. This

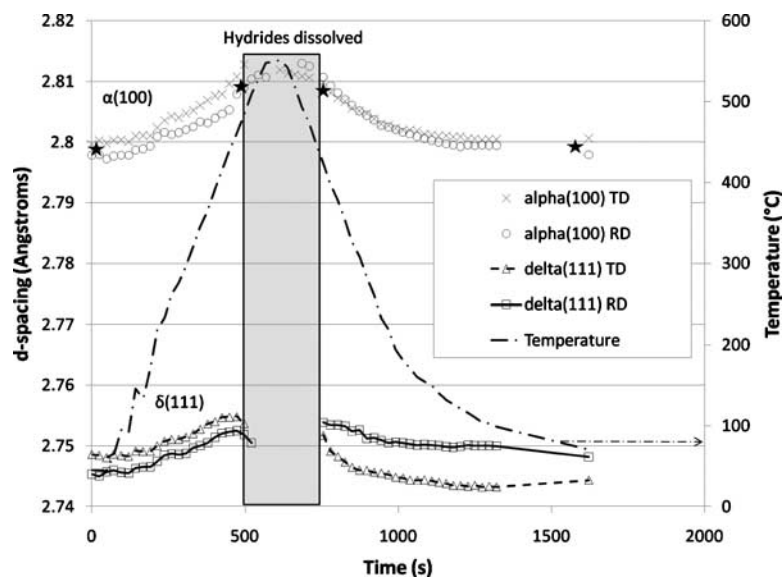


FIG. 13—The d -spacing of $\alpha(100)$ and $\delta(111)$ peaks for a Zircaloy-4 sample with 525 wt ppm of hydrogen cooled under 100 MPa applied load in the RD (the expected thermal expansion stars come from Ref 24). This cycle resulted in hydride reorientation.

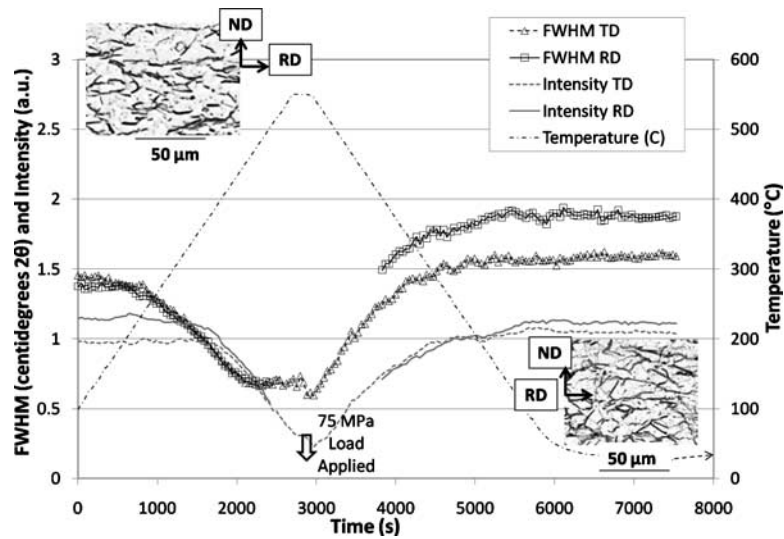


FIG. 14—Time evolution of the FWHM (and intensity) of the $\delta(111)$ peaks of a Zircaloy-4 sample with 525 wt ppm of hydrogen heated and cooled under 75 MPa applied load in the RD (no reorientation of hydrides). The applied load and temperature are also shown.

is likely due to strains developed during the hydride growth process due to the thermal expansion mismatch between the hydrides and the matrix. As the temperature decreases, the hydrides contract faster than the matrix, thus implying a higher strain on the precipitates and a higher strain broadening (the thermal expansion coefficient of the hydrides is $\alpha_{\text{hydrides}} = 14.2 \times 10^{-6} / ^\circ\text{C}$ and that of α -zirconium is $\alpha_{\text{Zr}} = 6 \times 10^{-6} / ^\circ\text{C}$ [18]). Once the load is applied in the RD, the FWHM in both directions increases as strain develops in the hydride particles in both the TD and the RD. Since the hydrides are under a tensile load in the RD, a TD strain results from Poisson's ratio, and thus both integration directions exhibit broadening. This broadening is likely tensile in the RD and compressive in the TD, although this cannot be readily determined from the diffraction peak widths.

Similar curves were plotted for samples cooled under 85 and 100 MPa, respectively, in Figs. 15 and 16. The analysis of the hydride peak intensities before and after heat treatment, performed using GSAS, shows that the diffracted intensities of the hydride peaks for the reoriented samples do not change significantly. The study of the peak shape (specifically peak broadening), however, was able to provide a

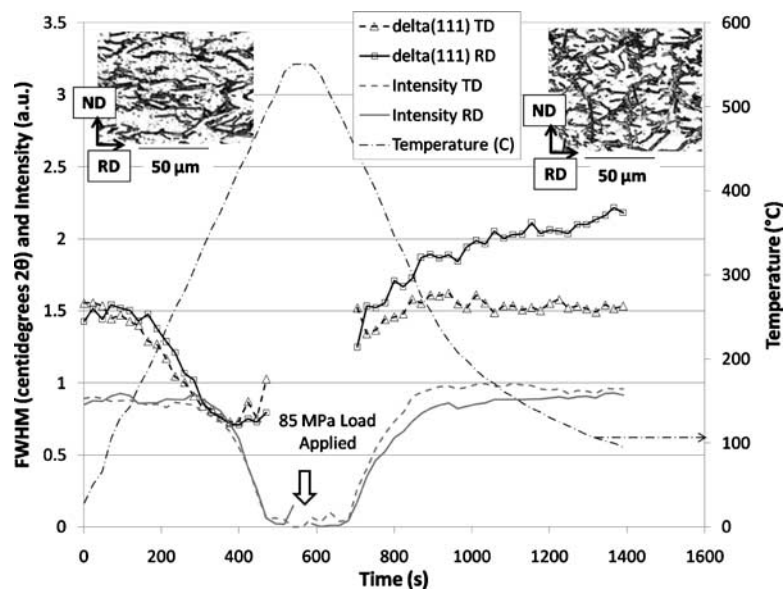


FIG. 15—Time evolution of the FWHM (and intensity) of the $\delta(111)$ peaks of a Zircaloy-4 sample with 525 wt ppm of hydrogen heated and cooled under 85 MPa applied load in the RD (this resulted in hydride reorientation). The applied load and temperature are also shown.

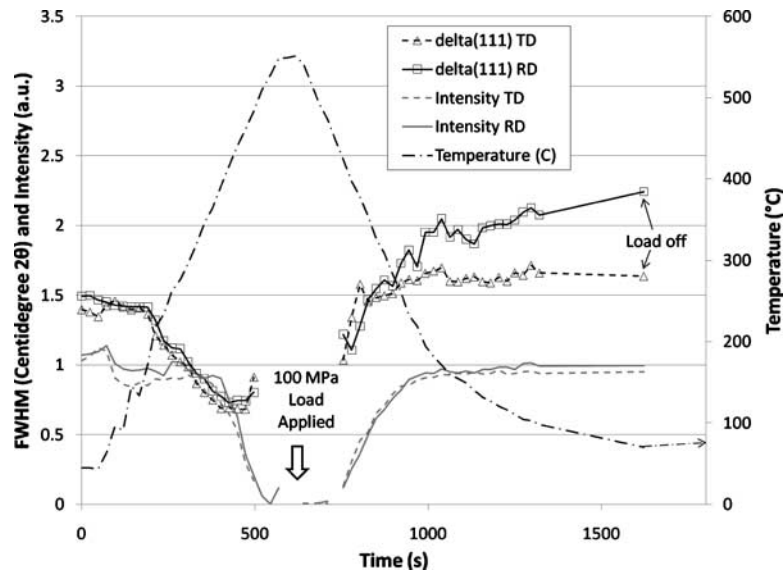


FIG. 16—Time evolution of the FWHM (and intensity) of the $\delta(111)$ peaks of a Zircaloy-4 sample with 525 wt ppm of hydrogen heated and cooled under 100 MPa applied load in the RD (this resulted in hydride reorientation). The applied load and temperature are also shown.

consistent “diffraction signature” associated with reoriented hydride particles. The metallographs taken before and after the 85 MPa experiment are represented in Fig. 15. Initially, the hydrides platelets are oriented in the circumferential direction with their normal parallel to ND. After the experiment (metallograph on the right-hand side of Fig. 15), some hydrides have reoriented and are now perpendicular to the load axis (which is the RD). Figure 15 shows that the hydride $(111)_\delta$ peak FWHM for the TD bank returns to its initial value after reprecipitation. However, for the peaks in the RD, the FWHM after reprecipitation is larger than previously and continues to increase as the temperature decreases below 150°C. This behavior is also observed for the sample held at 100 MPa (Fig. 16). This particular behavior of the RD bank of the hydrides is only observed in samples where hydride reorientation occurs and can therefore be considered a “signature” of reoriented hydride samples. The difference in the reoriented hydrides is that the broadening of the $(111)_\delta$ peak is *larger* in the RD than in the TD and increases continuously at the temperature decreases. We should note that the diffraction signal of the RD bank after hydride reorientation comes both from $(111)_\delta$ planes whose normals are *aligned* with the stress and planes whose normals are *perpendicular* to the applied stress. In contrast, the signal for the TD bank comes only from $(111)_\delta$ planes whose normal are perpendicular to the stress. As explained below, the peak broadening of the hydride peaks is likely due to strain broadening for the cases studied here. Since size broadening is shown not to be a factor (see next section), a plausible explanation for the broadening difference between the RD and the TD is that more strain (either plastic or elastic) is accumulated in the direction normal to the hydride platelet as it precipitates and grows than in the other direction. In fact, this is where the strain is most likely to accumulate during the plate-like precipitate growth [28]. The examination of Fig. 16 shows that even after the stress was removed towards the end of the run, the observed broadening remained, which suggests that the strain causing the broadening is likely *plastic* strain, likely in the form of dislocations, although there will also be a contribution from residual elastic strain (stress) due to the size and shape misfit between the precipitates and matrix.

Williamson–Hall Plots

The broadening observed in the previous graphs can be caused by several factors. Strain broadening and size broadening both could cause the broadening observed during our experiment (once instrumental broadening has been taken out). In order to quantitatively differentiate between strain and size broadening and to better understand the general state of strain of the hydrides, an analysis was carried out using Williamson–Hall plots [23]. The following relations allow us to distinguish between the two types of broadening [23]:

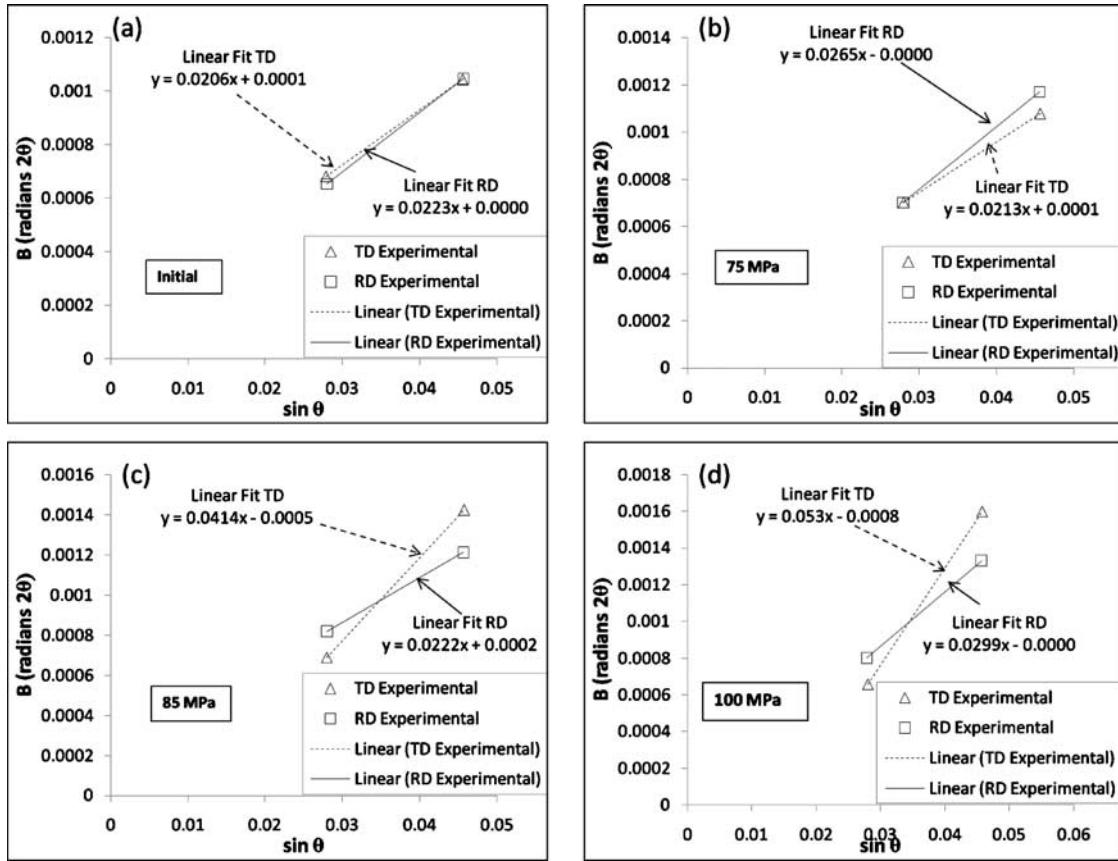


FIG. 17—Williamson–Hall plot for the final state of a Zircaloy-4 with 525 wt ppm of hydrogen heated up 550°C and cooled: (a) Under no load; (b) under 75 MPa applied load in the RD (no reorientation); (c) under 85 MPa applied load in the RD (hydride reorientation); and (d) under 100 MPa applied load in the RD (hydride reorientation).

$$\text{FWHM}_{\text{sample}} \propto \varepsilon \frac{\sin \theta}{\cos \theta} \quad \text{strain broadening} \quad (2)$$

$$\text{FWHM}_{\text{sample}} \propto \frac{0.9\lambda}{t \cos \theta} \quad \text{size broadening} \quad (3)$$

where:

$\text{FWHM}_{\text{Sample}}$ = measured FWHM minus the instrumental broadening (in radians 2θ),

θ = Bragg angle (in radians),

ε = lattice strain,

t = sample particle size (in nanometre), and

λ = X-ray beam wavelength (in nanometre).

A Williamson–Hall plot presents $\text{FWHM} \times \cos \theta$ (noted B) as a function of $\sin \theta$ for different peaks of the same phase. Strain broadening varies with the 2θ value of the peak under consideration, whereas size broadening is independent of angle when plotted in the Williamson–Hall plots. Therefore, the slope of the curves plotted is proportional to strain, and the y-intercept is proportional to the amount of size broadening [23]. A Williamson–Hall plot is presented in Fig. 17(a) for the same Zircaloy-4 sample as observed previously with 525 wt ppm of hydrogen for hydrides precipitated at slow cooling rate under no load and shown in Fig. 6. Only two, $(111)_{\delta}$ and $(220)_{\delta}$, out of the three hydride peaks are used in these graphs since the third hydride peak $(200)_{\delta}$ is too small and is highly convoluted with a very large α -zirconium peak and thus its shape cannot be fitted properly. By fitting the two points to a linear curve, we observe that the y-intercept is close to zero for both TD and RD. This implies that there is negligible size broadening of the hydride peaks. This is likely because the hydride particles we are detecting are too big to induce significant size broadening. The slopes of the fitted line in Fig. 17(a) are similar for both TD and RD. This is

consistent with the previous observation from the d -spacing calculation that both directions are strained to a similar amount, although the RD is slightly more strained than the TD (probably due to the presence of more basal planes of the zirconium matrix in the RD).

Figure 17(b) shows the Williamson–Hall plot for a diffraction pattern taken from a sample loaded at 75 MPa and taken at time $t=7500$ s, which corresponds to the final data point in Fig. 14. Similarly to Fig. 17(a), no hydride size broadening is observed in this sample. The slopes of the curve have increased slightly, suggesting that more strain accumulates in the hydrides as they are pulled in tension. Also, the hydride peaks in the RD seem to be more strained than the ones in the TD with a very large broadening of the $(220)_\delta$ peak. This means that the $(220)_\delta$ peaks oriented perpendicular to the loading direction are more strained than the $(111)_\delta$ peaks oriented in the same direction. This is likely due to different strain accommodation in the hydride platelet (the $(111)_\delta$ direction comes out of the hydride platelet).

Figure 17(c) and 17(d) shows Williamson–Hall plots for the 85 MPa and the 100 MPa reoriented samples, respectively. Again, no size broadening is observed. The analysis of the slopes from Fig. 17(c) and 17(d) compared to those in Fig. 17(a) suggests that the strain is larger on the TD than the RD (higher slope). This is paradoxical, considering the larger strain broadening observed in the $(111)_\delta$ in Figs. 15 and 16. However, because hydride reorientation was not complete (half of the hydrides present at the end are in-plane hydrides), it is likely that much of the $(220)_\delta$ peak intensity in the RD comes from in-plane hydrides. The analysis mentioned above is only properly valid if the same hydride particle contributes to the intensity of both $(111)_\delta$ and $(220)_\delta$. To summarize, the data is consistent with greater strain observed in the direction normal to the hydride platelets.

In summary, the observed strain in the direction normal to the hydrides platelets is likely caused by a combination of the accommodation of size-mismatch (volume expansion during hydride precipitation) and differential thermal expansion of the hydrides and matrix. The data collected in this study shows an identifiable diffraction signature for hydride reorientation. The main feature of this signature is that the FWHM continues to increase in the RD with time as the temperature decreases, whereas the FWHM remains unchanged in the TD. The second observation is that the strain in the TD is much higher than that in the RD. The d -spacing behavior of reoriented hydrides is the same as the behavior for samples under tensile stress without reorientation. This implies that this reorientation signature is not due to differences in the d -spacings but to another phenomenon. A possible explanation is that the diffraction signal from the $(220)_\delta$ peaks comes mostly from circumferential hydrides, whereas the diffraction signal from the $(111)_\delta$ peaks comes mostly from reoriented hydrides.

Conclusions

Detailed X-ray diffraction measurements were performed on various hydrided zirconium alloys samples using synchrotron radiation. The objective of the study was to understand the state of strain of hydrides as they precipitate in a zirconium matrix under load and when reorienting. The secondary objective of this study was to determine if there is a diffraction signature associated with hydride reorientation. Both in situ and ex situ experiments were performed on samples of different orientations, under different levels of load, and the results were compared to metallographical examination. The hydride strain was measured by comparing both d -spacing variations and the hydride peak broadening. The conclusions are as follows.

- (1) Hydrides particles precipitated under zero applied load are strained in compression in both directions (TD and RD), but the stresses remain in the elastic regime.
- (2) The analysis of the dependence of the observed hydride peak broadening on $\sin \theta$ indicates that most of the hydride peak broadening is caused by strain rather than by size. This is true both in the as-prepared hydrided samples and in those that underwent heat treatment and cooling under stress.
- (3) When hydrides are heated and stressed in the RD during cool-down but do not reorient, the peak FWHM in the TD and in the RD changes in a constant manner (i.e., reaches a plateau) relatively to the initial value. The variations in the hydride plane d -spacing are consistent with the planes whose normals are parallel to the loading axis (RD) being under tension and those whose normals are perpendicular to the loading axis (TD) being under compression.
- (4) A distinct diffraction signature associated with hydride reorientation has been identified for hydrided Zircaloy-4 samples, which are heated and cooled under stress applied in the RD. This signature is present only when the sample is cooled under an applied stress sufficient to reorient

hydrides. The FWHM of the $(111)_\delta$ hydride peaks in the RD and TD is markedly different in samples with reoriented hydrides compared to those in which reorientation did not occur. In samples where reorientation occurred, the FWHM of the $(111)_\delta$ peaks in the TD returns to the initial value upon cooling, while that for the RD increases steadily as temperature is lowered and precipitation proceeds. In contrast, in the non-reoriented samples, the FWHM of the $(111)_\delta$ peaks for both TD and RD return to the original value.

Acknowledgments

This research was funded by the Materials World Network Grant No. DMR-0710616 from the National Science Foundation, with corresponding funding from NSERC for the Canadian partners. The writers are grateful for their support. The research for this publication was supported by the Pennsylvania State University Materials Research Institute Nano Fabrication Network and the National Science Foundation Cooperative under Agreement No. 0335765, National Nanotechnology Infrastructure Network, with Cornell University. The use of the Advanced Photon Source was supported by the U.S. Department of Energy, Office of Basic Energy Sciences under Contract No. DE-AC02-06CH11357.

References

- [1] Coleman, C. E. and Hardie, D., "The Hydrogen Embrittlement of [Alpha]-Zirconium—A Review," *J. Less-Common Met.*, Vol. 11(3), 1966, pp. 168–185.
- [2] International Center for Diffraction Data, The Powder Diffraction File, Newton Square, PA, 2006.
- [3] Bradbrook, J. S., Lorimer, G. W., and Ridley, N., "The Precipitation of Zirconium Hydride in Zirconium and Zircaloy-2," *J. Nucl. Mater.*, Vol. 42(2), 1972, pp. 142–160.
- [4] Beck, R. L., "Zirconium-Hydrogen Phase System," *Transactions of the ASME*, Vol. 55, 1962, pp. 542–555.
- [5] Perovic, V., Weatherly, G. C., and Simpson, C. J., "Hydride Precipitation in [a]/[b] Zirconium Alloys," *Acta Metall.*, Vol. 31(9), 1983, pp. 1381–1391.
- [6] Chung, H. M., Daum, R. S., Hiller, J. M., and Billone, M. C., "Characteristics of Hydride Precipitation in Spent-Fuel Cladding," *Zirconium in the Nuclear Industry: 13th International Symposium, ASTM STP 918*, 2002, ASTM International, West Conshohocken, PA, pp. 78–101.
- [7] Eils, C. E., "Hydride Precipitates in Zirconium Alloys (A Review)," *J. Nucl. Mater.*, Vol. 28(2), 1968, pp. 129–151.
- [8] Kearns, J. J. and Woods, C. R., "Effect of Texture, Grain Size, and Cold Work on the Precipitation of Oriented Hydrides in Zircaloy Tubing and Plate," *J. Nucl. Mater.*, Vol. 20(3), 1966, pp. 241–261.
- [9] Singh, R. N., Kishore, R., Singh, S. S., Sinha, T. K., and Kashyap, B. P., "Stress-Reorientation of Hydrides and Hydride Embrittlement of Zr-2.5 wt% Nb Pressure Tube Alloy," *J. Nucl. Mater.*, Vol. 325(1), 2004, pp. 26–33.
- [10] Hardie, D. and Shanahan, M. W., "Stress Reorientation of Hydrides in Zirconium-2.5 % Niobium," *J. Nucl. Mater.*, Vol. 55(1), 1975, pp. 1–13.
- [11] Kammenzind, B. F., Berquist, B. M., Bajaj, R., Kreyns, P. H., and Franklin, D. G., "The Long-Range Migration of Hydrogen Through Zircaloy in Response to Tensile and Compressive Stress Gradients," *Zirconium in the Nuclear Industry: 12th International Symposium, ASTM STP 1354*, 2000, ASTM International, West Conshohocken, PA, pp. 196–233.
- [12] Daum, R. S., Chu, Y. S., and Motta, A. T., "Identification and Quantification of Hydride Phases in Zircaloy-4 Cladding Using Synchrotron X-Ray Diffraction," *J. Nucl. Mater.*, Vol. 392(3), 2009, pp. 453–463.
- [13] Kerr, M., Daymond, M. R., Holt, R. A., Almer, J. D., and Stafford, S., "Observation of Growth of a Precipitate at a Stress Concentration by Synchrotron X-Ray Diffraction," *Scr. Mater.*, Vol. 62(6), 2010, pp. 341–344.
- [14] Kerr, M., Daymond, M. R., Holt, R. A., Almer, J. D., Stafford, S., and Colas, K. B., "Fracture of a Minority Phase at a Stress Concentration Observed with Synchrotron X-Ray Diffraction," *Scr. Mater.*, Vol. 61(10), 2009, pp. 939–942.
- [15] Turski, M., Bouchard, P. J., Steuwer, A., and Withers, P. J., "Residual Stress Driven Creep Cracking

- in AISI Type 316 Stainless Steel,” *Acta Mater.*, Vol. 56, 2008, pp. 3598–3612.
- [16] Daymond, M. R., Young, M. L., Almer, J. D., and Dunand, D. C., “Strain and Texture Evolution During Mechanical Loading of a Crack Tip in Martensitic Shape-Memory NiTi,” *Acta Mater.*, Vol. 55(3929), 2007, pp. 3929–3942.
- [17] Pierron, O. N., Koss, D. A., Motta, A. T., and Chan, K. S., “The Influence of Hydride Blisters on the Fracture of Zircaloy-4,” *J. Nucl. Mater.*, Vol. 322(1), 2003, pp. 21–35.
- [18] Douglass, D. L., “The Metallurgy of Zirconium,” *Atomic Energy Review*, Z. I. Turkov, Ed., International Atomic Energy Agency, Vienna, Austria, 1971.
- [19] Raynaud, P. A. C., *Crack Growth Through the Thickness of Thin-Sheet Hydrided Zircaloy-4*, Ph.D. Thesis, The Pennsylvania State University, University Park, 2009.
- [20] McMinn, A., Darby, E. C., and Schofield, J. S. “The Terminal Solid Solubility of Hydrogen in Zirconium Alloys,” *Zirconium in the Nuclear Industry: 12th International Symposium, ASTM STP 1354*, 2000, ASTM International, West Conshohocken, PA, pp. 173–195.
- [21] Haeffner, D. R., Almer, J. D., and Lienert, U., “The Use of High Energy X-Rays from the Advanced Photon Source to Study Stresses in Materials,” *Mater. Sci. Eng., A*, Vol. 399(1–2), 2005, pp. 120–127.
- [22] Larson, A. C. and Von Dreele, R. B., *General Structure Analysis System (GSAS)*, Los Alamos National Laboratory, Los Alamos, NM, Report LAUR 86-748, 2000.
- [23] Snyder, R. L., Fiala, J., and Bunge, H., *Defect and Microstructure Analysis by Diffraction*, International Union of Crystallography Monographs on Crystallography, Oxford University Press, New York, NY, 1999.
- [24] Puls, M. P., Shi, S.-Q., and Rabier, J., “Experimental Studies of Mechanical Properties of Solid Zirconium Hydrides,” *J. Nucl. Mater.*, Vol. 336(1), 2005, pp. 73–80.
- [25] Yamanaka, S., Yamada, K., Kurosaki, K., Uno, M., Takeda, K., Anada, H., Matsuda, T., and Kobayashi, S., “Characteristics of Zirconium Hydride and Deuteride,” *J. Alloys Compd.*, Vol. 330–332, 2002, pp. 99–104.
- [26] Kerr, M., Daymond, M. R., Holt, R. A., and Almer, J. D., “Strain Evolution of Zirconium Hydride Embedded in a Zircaloy-2 Matrix,” *J. Nucl. Mater.*, Vol. 380(1–3), 2008, pp. 70–75.
- [27] Yamanaka, S., Yoshioka, K., Uno, M., Katsura, M., Anada, H., Matsuda, T., and Kobayashi, S., “Thermal and Mechanical Properties of Zirconium Hydride,” *J. Alloys Compd.*, Vol. 293–295, 1999, pp. 23–29.
- [28] Massih, A. R. and Jernkvist, L. O., “Stress Orientation of Second-Phase in Alloys: Hydrides in Zirconium Alloys,” *Comput. Mater. Sci.*, Vol. 46, 2009, pp. 1091–1097.